


Mineralization of the Luanling gold deposit in the southern margin of the North China Craton: Insights from mineralogy and mineral chemistry of sulfides, tellurides and oxides

Lei Meng^{1,2}  | Xin-Yu Gao¹ | Qiang Wu^{1,2} | Tai-Ping Zhao¹ 

¹Key Laboratory of Mineralogy and Metallogeny, Guangzhou Institute of Geochemistry, Chinese Academy of Sciences, Guangzhou, China

²University of Chinese Academy of Sciences, Beijing, China

Correspondence

Tai-Ping Zhao, Key Laboratory of Mineralogy and Metallogeny, Guangzhou Institute of Geochemistry, Chinese Academy of Sciences, Guangzhou, China.
Email: tpzhao@gig.ac.cn

Funding information

National Key Research and Development Program of China, Grant/Award Number: No.2016YFC0600106; National Natural Science Foundation of China, Grant/Award Number: Nos. 41373046 & 41402047

Handling Editor: S-R. Li

The Luanling gold deposit, a typical Te-Au deposit in the Xiong'er terrane, the southern margin of the North China Craton, contains two types of ores, namely altered rock-type and quartz vein-type ores. Gold is hosted by pyrite and As-bearing pyrite in the altered rock-type ores, whereas tellurides are the main gold carriers in the quartz vein-type ores. In order to investigate their origins, we calculated the Gibbs free energies of formation and reaction of related sulfides, tellurides and oxides from different ore types. The phase diagrams of these minerals were constructed at 300 °C, a temperature at which gold was mainly precipitated in the Luanling deposit. According to phase relations among sulfides, $\log fS_2(g)$ is constrained between -10.4 and -6.5 . In addition, we propose that $[Au(HS)_2]^-$ was the dominant carrier of gold in ore-forming fluid, and its decomposition formed pyrite and arsenian pyrite, in which gold mainly exists as an invisible phase. In the quartz vein-type ores, $\log fTe_2(g)$ and $\log fO_2(g)$ are constrained to range from -13.68 to -7.9 and -36.8 to -31.1 , respectively, based on the phase relations between tellurides, sulfides and oxides, and gold was mainly transported as $[Au(HTe)_2]^-$ and its break down formed gold-bearing, including sylvanite, petzite and Au-Ag-tellurides. Sylvanite and petzite, the two stable Au-Ag tellurides, were probably precipitated primarily from hotter ore-forming fluids. According to phase relations among tellurides, the two phases were decomposed into native gold, hessite and more stable Au-Ag-tellurides with the changes of physicochemical conditions in the later stages. In addition, we proposed that the ore-forming fluids relevant to the altered rock- and the quartz vein-type ores were from the same source and continuously evolved.

KEYWORDS

gold mineralization, Luanling gold deposit, southern margin of the North China Craton, sulfides, tellurides

1 | INTRODUCTION

Sulfides, especially pyrite, arsenian pyrite and arsenopyrite, are usually major carriers of gold in gold deposits (Afifi, Kelly, & Essene, 1988a; Simon, Huang, et al., 1999; Deditius et al., 2008; Xu et al., 2014;

Zhou et al., 2018; Liu et al., 2019). Compared with the above-mentioned sulfides, tellurides are commonly rare in gold deposits, but they can also be important carriers of Au, Ag and platinum-group elements (PGE) (Afifi et al., 1988a; Afifi, Kelly, & Essene, 1988b; Cabri, 1965; Ciobanu et al., 2006 and references therein). Due to the similar

geochemical behaviour between Te and S, Te could enter into the lattice of sulfides via isomorphism substitution (Ciobanu et al., 2006), and tellurides are commonly associated with sulfides, oxides and/or native elements (Au, Ag etc.) in natural deposits (Afifi et al., 1988a, 1988b). Comprehensive experiments and calculations have been carried out to investigate relative stabilities of tellurides, sulfides, oxides, selenides and native elements and to build phase relations among these minerals and/or elements (Afifi et al., 1988a, 1988b; Cabri, 1965; Holland, 1959, 1965; Liu et al., 2000; Simon & Essene, 1996; Simon et al., 1997 and references therein), indicating that the stability of these minerals are sensitive to a series of physicochemical parameters, especially temperature and fugacities of tellurium, sulfur, oxygen and selenium. Nevertheless, the majority of previous studies primarily focused on the thermodynamic properties of tellurides, sulfides, oxides and selenides, but rare studies applied phase relations among these minerals to investigate ore-forming processes.

Large amounts of gold deposits, especially the altered-type gold deposits, are developed in the Xiong'er terrane, the southern margin of the North China Craton (Li & Santosh, 2014, 2017; Yang & Santosh, 2020; Zhao et al., 2018 and references therein). Telluride minerals have been reported in several deposits, such as Shanggong, Qiyugou, Beiling, Luanling and Qianhe (Chao et al., 2016; Chen et al., 1999; Tang et al., 2013). Among them, the Luanling gold deposit is a typical Te-Au deposit with middle-scale and contains two types of ores, the altered rock- and quartz vein-type ores. In the altered rock-type ores, gold mainly occurs as invisible phase in pyrite and arsenian pyrite, while in the quartz vein-type ores, tellurides are the dominated gold-bearing phases. Some studies have been conducted on the mineralization timing, mineral assemblages and origin of the Luanling gold deposit (Chao et al., 2016; Wang et al., 2011). However, the issue related to the ore-forming processes remains poorly constrained. Therefore, in order to better understand the ore-forming process for the two different types of ores, we carried out detailed studies on the mineralogy and phase equilibria based on relative stabilities of sulfides, tellurides and oxides. This study sheds new lights on the origin of the diversity of gold mineralization in this deposit.

2 | GEOLOGIC BACKGROUND

2.1 | Geology of the Xiong'er terrane

The Xiong'er terrane is located in the southern margin of the North China Craton (Li & Santosh, 2017; Gao et al., 2010; Zhao et al., 2018; Figure 1b). It is geologically defined by the Machaoying Fault to the south and the Luoning detachment Fault to the north (Tang et al., 2013 and references therein; Figure 1c). A number of secondary NNE-NE-trending faults are spaced with near equal intervals, and the occurrence of ore deposits are controlled by these faults in the Xiong'er terrane (Chen et al., 2006, 2008; Figure 1c). The Xiong'er terrane is lithologically composed of the late Archean to early Paleoproterozoic Taihua Group

(2.5–2.3Ga; Xue et al., 1995; Xu et al., 2009) and the unconformably overlying Paleoproterozoic Xiong'er Group (1.80–1.75Ga; Zhao et al., 2004). The Taihua Group consists chiefly of sillimanite-garnet gneiss, graphite gneiss, TTG gneiss, migmatite, amphibolite, marble, and metamorphosed supracrustal rocks intercalated with mafic to ultramafic rocks (Hu et al., 1988; Xu et al., 2009). The Xiong'er Group mainly comprises basaltic andesite, andesite and minor dacitic-rhyolitic rocks (Zhao et al., 2007). Mesoproterozoic to Neoproterozoic sedimentary sequences, unconformably overlying the Xiong'er Group (Chen et al., 2006; Figure 1c), are well developed in the south of the Machaoying Fault, including the Guandaokou and Luanchuan groups. The Songxian-Jiuxian and Yiyang-Luoning-Lushi rift basins, located to the east and west of the Xiong'er terrane, develop Cretaceous-Quaternary sedimentary rocks (Hu et al., 1988).

The late Mesozoic magmatic intrusions are widely distributed in the Xiong'er terrane (Gao & Zhao, 2017), including the Wuzhangshan pluton (156.8±1.2Ma, Mao et al., 2010), Huashan pluton (128 to 132Ma, Mao et al., 2010; Xiao et al., 2012) and Heyu plutons (148 to 127Ma, Guo et al., 2009; Gao et al., 2010; Mao et al., 2010) (Figure 1c). The formation of the late Mesozoic granitic intrusions were proposed to be related either with the Mesozoic collisions leading to formation of the Qinling Orogeny (Bao et al., 2016; Chen & Fu, 1992; Xiao et al., 2012), or the destruction of the North China Craton (Gao et al., 2017; Zhu et al., 2011; Zhao et al., 2018).

2.2 | Geology of the Luanling gold deposit

The late Mesozoic Mo-Au-Pb-Zn-Ag mineralization are pervasively developed in the Xiong'er terrane (Zhao et al., 2018 and references therein). The gold mineralization, in particular, is mainly altered rock-type with minor quartz vein- and breccia-type gold deposits (Li & Santosh, 2014; Zhao et al., 2018 and references therein). The Luanling gold deposit is a typical Te-Au deposit in the Xiong'er terrane (Chao et al., 2016). The deposit has a proven and probable reserve of 5t Au, with an average grade of ~4.8g/t. In this deposit, ore bodies are hosted by the iron-rich trachyandesite and andesite of the Xiong'er Group. The NW-trending faults of F1 and F2 are the main structures, and higher-order ore-controlled faults are widely developed in the mining district, including F911, F912, F971, F972 and F976 (260–1200m long and ~0.2–2.2m wide) (Figure 2a). Re-Os isochron age of molybdenite associated with Au-bearing minerals indicates that the gold mineralization occurred at 163±2Ma (Chao et al., 2016). The ores in the Luanling gold deposit can be divided into two typical sub-types, the altered rock- (Figure 3a) and quartz vein-type ores (Figure 3b). The altered rock-type ores usually occurs along both sides of, and sometimes as inclusions in the quartz vein-type ores (Figure 3b). These observations indicate that the quartz vein-type ores were slightly preceded by the altered rock-type ores.

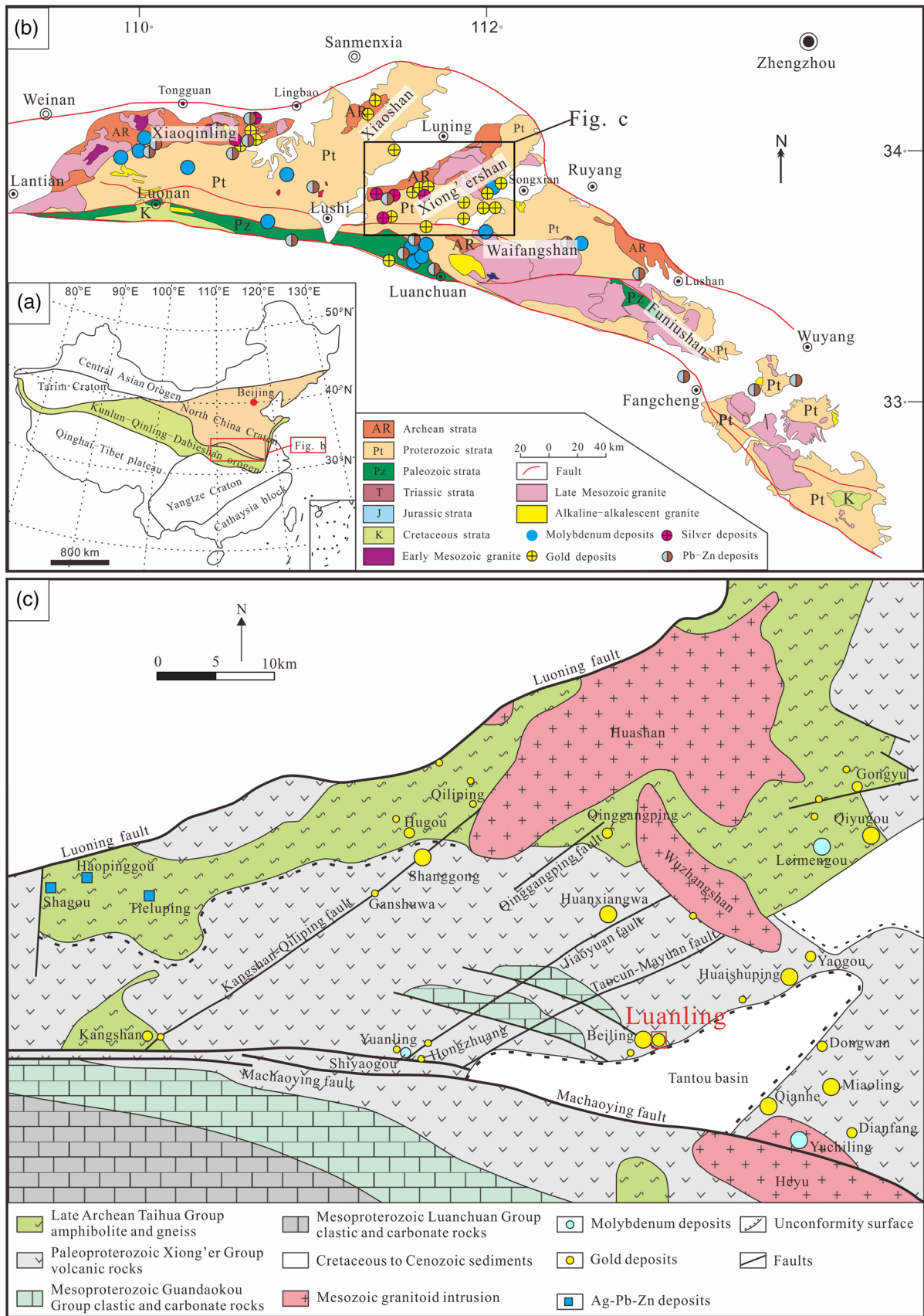
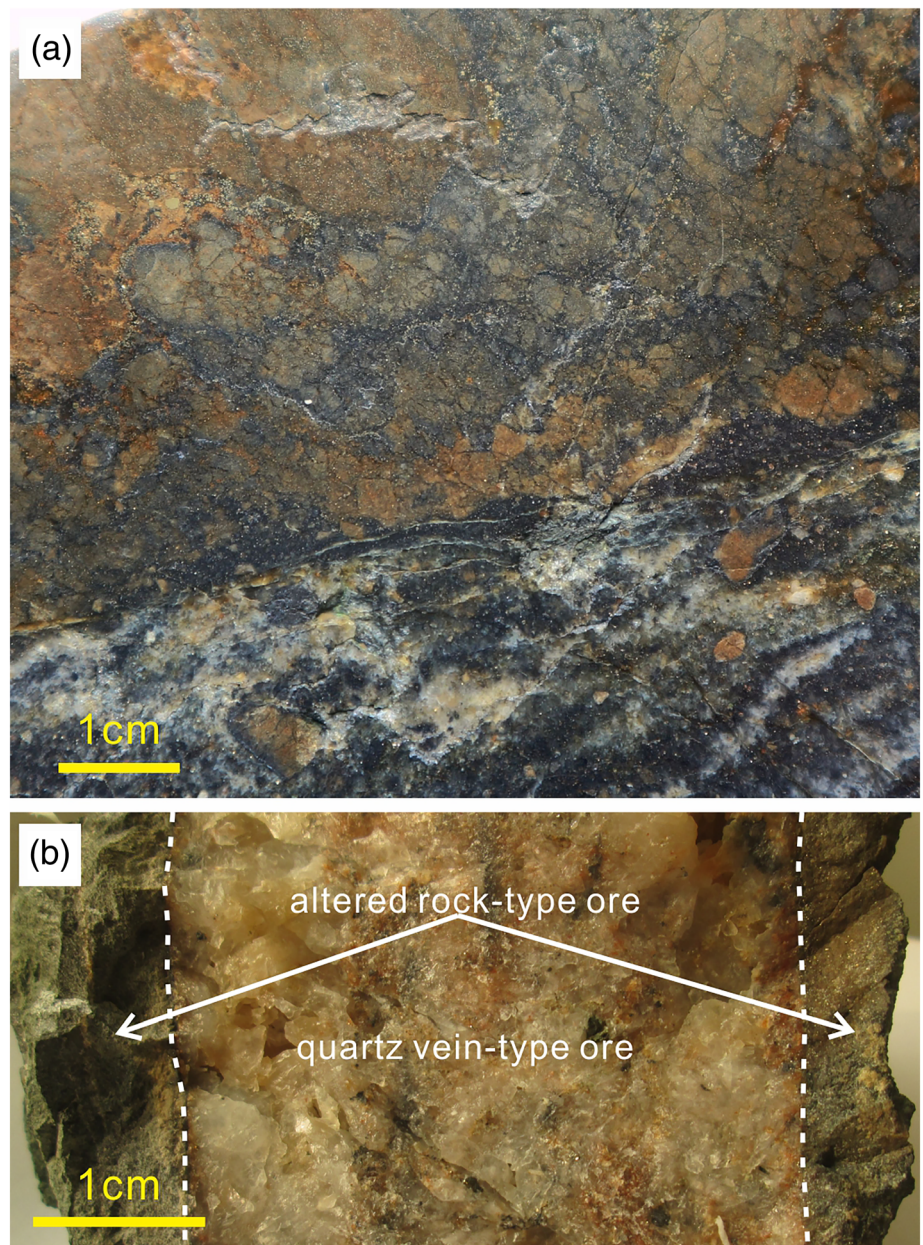


FIGURE 1 (a) Major Tectonic outlines of China and (b) tectonic setting of the southern margin of the North China Craton, modified after Zhao et al. (2018); (c) geological and tectonic map of the Xiong'er terrane and the location of the Luanling gold deposit, modified after Lu et al. (2004) [Colour figure can be viewed at wileyonlinelibrary.com]

FIGURE 3 Photographs of (a) the altered rock-type ores and (b) quartz vein-type ores [Colour figure can be viewed at wileyonlinelibrary.com]



This deposit mainly comprises K-feldspar, quartz, sulfide, sericite, carbonate and chlorite alteration (Chao et al., 2016; Wang et al., 2011). Based on the detailed petrographic observations and the crosscutting relationships, the mineralization of this deposit involves three stages, including early stage (E), main mineralization stage (M) and late stage (L) (Figure 4).

The E stage is dominated by quartz and K-feldspar, with minor barite and ankerite (Chao et al., 2016). The M stage is the main mineralization stage, which formed two sub-types of ores during this stage, including altered rock- and quartz vein-type ores. In the altered rock-type ores, the ore minerals are mainly pyrite and arsenian pyrite (Figure 5), with minor galena, sphalerite, chalcopyrite and molybdenite (Wang et al., 2011). In addition, gold predominantly occurs as invisible phase in arsenian pyrite and pyrite, which

were disseminated in the altered rock-type ores. (Figure 3a). Gangue minerals are dominated by quartz and sericite with rare monazite and barite.

The quartz vein-type ores is characterized by tellurides and sulfides. Furthermore, tellurides are the major Au-bearing phases, including calaverite, petzite, hessite and altaite (Table 2). Sulfides are the subordinate Au-bearing minerals, including bornite, enargite, tetrahedrite, Zn-bearing tetrahedrite, Zn-bearing tennantite and pyrite (Table 2). Gold minerals generally occur as inclusions or microfracture-infills in quartz, sphalerite and bornite (Figures 5h, l and 6) (Chao et al., 2016). The L stage contains quartz and calcite with trace amounts sericite. Besides, the L stage veinlets penetrate quartz-sericite-sulfides vein of the M stage (Chao et al., 2016).

Stage Mineral	Early	Main		Late
		Altered rock-type ores	Quartz vein-type ores	
Quartz				
K-feldspar				
Barite	?			
Calcite				
Sericite				
Chlorite				
Pyrite				
As-pyrite				
Molybdenite				
Sphalerite				
Galena				
Chalcopyrite				
Bornite				
Enargite				
Tetrahedrite				
Tennantite				
Digenite				
Anilite				
Petzite				
Calaverite				
Hessite				
Altaite				
Native gold				
Native tellurium				?

FIGURE 4 Paragenetic sequence of minerals in the Luanling gold deposit

3 | ANALYTICAL METHODS

Petrological features and chemical compositions of sulfides, tellurides and oxides were determined by scanning electron microscopes (SEM, SUPRA 55 SAPPHIRE, ZEISS Company, Germany) with energy spectrometer (EDS) and electron microprobe analysis (EMPA, JXA-8230, JEOL Company, Japan), respectively. The SEM and EMPA analyses were carried out at the Guangzhou Institute of Geochemistry, Chinese Academy of Sciences and the Department of Earth Sciences, University of Hong Kong, respectively. X-ray lines, used for EMPA analyses, were listed as following: Co (K_{α}), Hg (L_{α}), Sb (L_{α}), As (L_{α}), Fe (K_{α}), Au (M_{α}), Ni (K_{α}), Cu (K_{α}), Zn (K_{α}), S (K_{α}), Pb (M_{α}), Bi (M_{α}), Ag (L_{α}), Te (L_{α}) and Se (L_{α}). The analyses were performed under an acceleration voltage of 20kV and beam current of 20nA with wavelength dispersive X-ray spectrometers (WDS). The electron beam is 1 μ m in diameter. In order to improve the statistics of the count rates, peak counting times were 20s for Fe, Te and S, 40s for As and Cu, 60s for Pb, Zn, Ni, Co, Hg, Sb, Au, Bi, Ag and Se. Standard specimens used for calibration were Co⁰ (for Co), FeS₂ (for S), Sb⁰ (for Sb), FeAsS (for As), FeS₂ (Fe), Au⁰ (for Au), Ni⁰ (for Ni), CuFeS₂ (for Cu), ZnS (for Zn), FeS₂ (for S), Pb⁰ (for Pb), Bi⁰ (for Bi), Ag⁰ (for Ag), Te⁰ (for Te) and Se⁰ (Se).

4 | MINERALOGY AND MINERAL CHEMISTRY

4.1 | Pyrite and arsenian pyrite in altered rock-type ores

EMP analyses of the sulfides in the altered rock-type ores show that gold predominantly occurs as invisible Au in pyrite and arsenian pyrite (Table 1). The arsenian pyrite contains 0.73 to 8.78 wt.% Au and 100 to 1200 ppm As, respectively, while Cu (0.01 ~ 4.03 wt.%) and Se (below detection to 0.21 wt.%) contents in arsenian pyrite are variable. Besides, tellurides are not detected in this type of ore.

4.2 | Sulfides in quartz vein-type ores

Sulfides are abundant in quartz vein type ores, which mainly comprise sphalerite, galena and Cu-chalcogenides (Figures 5 and 6). The Cu-chalcogenides are mainly composed of bornite and chalcopyrite and contain rare digenite, anilite, enargite, tetrahedrite and intergrown with tellurides, especially hessite and altaite (Figure 5). Some digenite generally occurs along the rim of bornite,

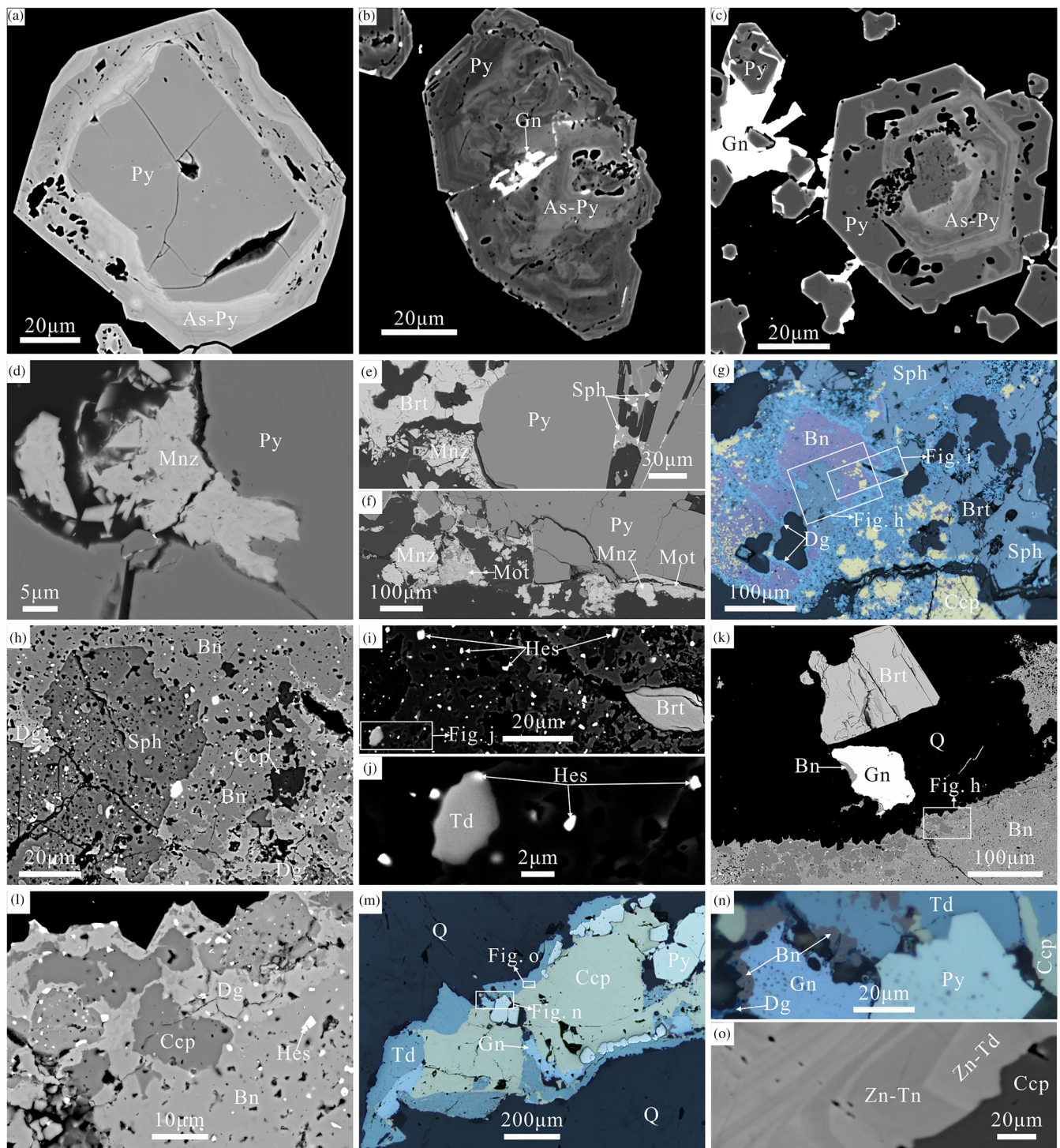


FIGURE 5 Backscattered electron images of sulfides in the altered rock- (a-c) and quartz vein-type ores (d-o). (a) Pyrite is surrounded by arsenian pyrite. (b) Galena occurs as inclusions in the arsenian pyrite. (c) Pyrite is cemented by galena. (d-f) Intergrowths of pyrite, monazite, barite, molybdenite and sphalerite; (g-h) Bornite and chalcopyrite are associated with sphalerite and replaced by digenite. (i) Hessite and barite occur as inclusions in bornite. (j) Tetrahedrite coexisting with hessite. (k) Intergrowths of bornite, galena, barite and chalcopyrite. (l) Digenite replacing chalcopyrite and bornite. (m-n) Intergrowths of galena, pyrite, chalcopyrite and tetrahedrite. (o) Exsolution of Zn-bearing tennantite in tetrahedrite. Py: pyrite, As-Py: As-bearing pyrite, Gn: galena, Mnz: monazite, Brt: barite, Sph: sphalerite, Bn: bornite, Mot: molybdenite, Dg: digenite, Ccp: chalcopyrite, Hes: hessite, Zn-Td: Zn-bearing tetrahedrite, Zn-Tn: Zn-bearing tennantite [Colour figure can be viewed at wileyonlinelibrary.com]

with irregular/corrosive contacts between the digenite and bornite (Figure 5g, h, l), which indicates that the digenite may result from dissociation and replacement of bornite. Observed

intergrowth pairs comprise: (a) chalcopyrite-bornite-sphalerite-hessite (Figure 5e); (b) tetrahedrite-hessite (Figure 5g); (c) bornite-galena (Figure 5h); (d) chalcopyrite-bornite-digenite-hessite

TABLE 1 EMPA data (wt.%) of sulfides in the altered rock-type ores from the Luanling gold deposit

Number	Mineral	Se	Hg	S	Pb	Zn	Cu	Ni	Co	As	Fe	Au	Ag	Sb	Te	Total
D03	Py	0.18	b.d.l.	52.82	b.d.l.	b.d.l.	0.03	b.d.l.	0.05	0.18	45.96	0.03	b.d.l.	b.d.l.	b.d.l.	99.25
D05	Py	0.01	b.d.l.	53.00	b.d.l.	b.d.l.	b.d.l.	b.d.l.	0.14	b.d.l.	46.00	b.d.l.	b.d.l.	b.d.l.	b.d.l.	99.15
D08	Py	0.03	b.d.l.	52.89	b.d.l.	b.d.l.	0.07	0.01	1.75	b.d.l.	44.32	b.d.l.	b.d.l.	b.d.l.	b.d.l.	99.08
D10	Py	b.d.l.	b.d.l.	53.22	b.d.l.	0.01	b.d.l.	b.d.l.	0.05	b.d.l.	45.87	b.d.l.	b.d.l.	b.d.l.	b.d.l.	99.16
D15	Py	b.d.l.	b.d.l.	53.24	b.d.l.	b.d.l.	b.d.l.	b.d.l.	0.05	b.d.l.	46.26	b.d.l.	b.d.l.	b.d.l.	b.d.l.	99.55
D22	Py	0.15	b.d.l.	52.97	b.d.l.	b.d.l.	0.01	0.02	0.05	b.d.l.	46.18	b.d.l.	0.01	b.d.l.	b.d.l.	99.38
D11	Py	b.d.l.	b.d.l.	53.03	b.d.l.	0.01	0.57	0.28	0.16	0.07	45.02	0.03	b.d.l.	b.d.l.	b.d.l.	99.17
D12	Py	b.d.l.	b.d.l.	53.20	b.d.l.	b.d.l.	0.03	b.d.l.	0.05	0.01	46.03	0.02	b.d.l.	b.d.l.	b.d.l.	99.34
D72	Py	b.d.l.	b.d.l.	52.57	b.d.l.	0.02	b.d.l.	b.d.l.	0.04	0.43	46.31	0.02	b.d.l.	b.d.l.	b.d.l.	99.38
D01	As-Py	b.d.l.	b.d.l.	47.76	b.d.l.	0.01	0.04	b.d.l.	0.05	6.99	44.00	0.12	b.d.l.	0.01	b.d.l.	98.98
D04	As-Py	0.21	b.d.l.	47.56	b.d.l.	0.01	0.03	b.d.l.	0.05	7.36	43.80	0.10	b.d.l.	0.03	b.d.l.	99.15
D06	As-Py	b.d.l.	b.d.l.	48.26	b.d.l.	b.d.l.	0.03	b.d.l.	0.07	6.95	44.09	0.05	0.01	0.06	b.d.l.	99.52
D09	As-Py	b.d.l.	b.d.l.	48.85	b.d.l.	b.d.l.	0.27	b.d.l.	0.08	6.29	44.33	0.02	b.d.l.	b.d.l.	b.d.l.	99.88
D41	As-Py	b.d.l.	b.d.l.	51.98	b.d.l.	b.d.l.	0.98	b.d.l.	0.04	1.92	44.15	0.02	0.02	b.d.l.	0.12	99.23
D43	As-Py	0.14	b.d.l.	51.75	b.d.l.	b.d.l.	1.16	b.d.l.	0.03	2.04	44.03	0.02	0.03	0.01	0.11	99.32
D44	As-Py	b.d.l.	b.d.l.	51.56	0.04	b.d.l.	4.03	b.d.l.	0.03	1.50	41.05	0.02	0.08	b.d.l.	0.74	99.05
D48	As-Py	b.d.l.	b.d.l.	51.59	b.d.l.	b.d.l.	0.94	b.d.l.	0.05	2.07	44.64	0.02	b.d.l.	0.00	0.10	99.40
D73	As-Py	b.d.l.	b.d.l.	46.65	0.38	b.d.l.	0.34	b.d.l.	0.05	8.78	42.22	0.09	0.03	0.34	b.d.l.	98.87
D13	Gn	b.d.l.	b.d.l.	12.79	86.72	b.d.l.	b.d.l.	b.d.l.	b.d.l.	b.d.l.	0.75	b.d.l.	b.d.l.	b.d.l.	0.03	100.33
D75	Gn	b.d.l.	b.d.l.	13.36	86.02	b.d.l.	b.d.l.	b.d.l.	b.d.l.	b.d.l.	0.04	b.d.l.	b.d.l.	b.d.l.	b.d.l.	99.43

Abbreviation: b.d.l., below detection limit.

TABLE 2 EMPA data (wt.%) of sulfides and tellurides in the quartz vein-type ores from the Luanling gold deposit

Number	Mineral	Se	Hg	S	Pb	Zn	Cu	Ni	Co	As	Fe	Au	Ag	Sb	Te	Total
D36	Py	b.d.l.	b.d.l.	52.22	b.d.l.	b.d.l.	0.62	b.d.l.	0.05	0.46	45.31	0.02	0.01	b.d.l.	0.03	98.71
D37	Py	b.d.l.	b.d.l.	51.87	b.d.l.	b.d.l.	1.32	b.d.l.	0.04	0.43	45.06	0.02	0.01	b.d.l.	0.02	98.76
D38	Py	b.d.l.	b.d.l.	52.39	0.05	b.d.l.	0.41	b.d.l.	0.04	0.56	45.41	0.02	0.03	0.05	0.04	99.00
D40	Py	0.01	b.d.l.	52.22	b.d.l.	b.d.l.	2.15	b.d.l.	0.04	0.52	44.16	b.d.l.	0.01	b.d.l.	0.10	99.19
D45	Py	0.01	b.d.l.	52.86	b.d.l.	b.d.l.	2.27	b.d.l.	0.04	0.16	43.87	b.d.l.	0.00	b.d.l.	0.07	99.30
D46	Py	b.d.l.	b.d.l.	52.73	b.d.l.	b.d.l.	0.31	b.d.l.	0.04	0.33	45.76	0.02	0.00	b.d.l.	0.05	99.23
D59	Py	b.d.l.	b.d.l.	53.24	b.d.l.	b.d.l.	0.07	b.d.l.	0.03	b.d.l.	46.41	b.d.l.	0.00	b.d.l.	b.d.l.	99.75
D49	Gn	b.d.l.	0.07	12.60	87.10	0.05	0.51	b.d.l.	b.d.l.	b.d.l.	0.11	b.d.l.	0.00	b.d.l.	0.02	100.44
D57	Gn	b.d.l.	b.d.l.	13.27	81.08	0.98	5.18	0.01	b.d.l.	b.d.l.	0.30	b.d.l.	0.00	0.49	b.d.l.	101.31
D58	Gn	0.20	b.d.l.	12.90	86.14	b.d.l.	0.43	b.d.l.	b.d.l.	b.d.l.	0.34	b.d.l.	0.00	b.d.l.	0.03	100.06
D75	Gn	0.00	b.d.l.	13.36	86.02	b.d.l.	b.d.l.	b.d.l.	b.d.l.	b.d.l.	0.04	b.d.l.	0.00	b.d.l.	b.d.l.	99.43
D53	Ccp	0.34	b.d.l.	34.54	b.d.l.	0.03	34.26	b.d.l.	0.02	b.d.l.	29.98	b.d.l.	0.01	b.d.l.	b.d.l.	99.18
D257	Sp	0.01	b.d.l.	32.40	b.d.l.	64.30	0.93	b.d.l.	b.d.l.	0.01	0.26	b.d.l.	0.00	b.d.l.	0.02	97.93
D55	Bn	0.23	b.d.l.	25.74	b.d.l.	0.15	60.61	b.d.l.	0.02	b.d.l.	12.56	b.d.l.	0.04	0.09	b.d.l.	99.46
D56	Bn	0.14	b.d.l.	24.97	0.02	0.08	61.02	b.d.l.	0.02	b.d.l.	11.12	b.d.l.	0.05	b.d.l.	b.d.l.	97.42
D56-1	Bn	0.13	b.d.l.	26.23	0.02	0.08	61.11	b.d.l.	0.02	b.d.l.	11.16	b.d.l.	0.05	b.d.l.	b.d.l.	98.80
D64	Bn	b.d.l.	b.d.l.	26.21	0.03	0.15	61.56	b.d.l.	b.d.l.	b.d.l.	10.76	b.d.l.	0.09	b.d.l.	b.d.l.	98.80
D71	Bn	b.d.l.	0.01	26.53	0.08	0.14	61.31	b.d.l.	0.01	b.d.l.	10.71	b.d.l.	0.13	b.d.l.	b.d.l.	98.92
D60	Enr	b.d.l.	b.d.l.	28.41	0.16	6.29	43.92	0.01	0.02	16.00	3.84	b.d.l.	0.08	1.68	b.d.l.	100.40
D61	Enr	b.d.l.	0.05	27.46	0.57	7.18	42.90	b.d.l.	0.01	18.77	1.06	b.d.l.	0.24	1.31	b.d.l.	99.55
D62	Enr	b.d.l.	b.d.l.	27.38	0.50	6.61	45.46	b.d.l.	0.02	15.71	2.89	b.d.l.	0.16	1.50	b.d.l.	100.22
D63	Enr	b.d.l.	b.d.l.	32.06	b.d.l.	0.29	47.50	b.d.l.	b.d.l.	18.27	0.69	b.d.l.	0.02	0.41	b.d.l.	99.27
D65	Enr	b.d.l.	b.d.l.	27.42	0.14	7.51	42.21	b.d.l.	0.01	18.72	1.17	b.d.l.	0.05	1.92	b.d.l.	99.16
D66	Enr	b.d.l.	b.d.l.	32.12	b.d.l.	0.27	47.76	b.d.l.	b.d.l.	18.41	0.69	b.d.l.	0.01	0.47	b.d.l.	99.74
D39	Td	b.d.l.	b.d.l.	30.62	0.65	b.d.l.	23.04	b.d.l.	0.02	3.00	8.85	0.03	0.02	34.61	b.d.l.	100.85
D39-1	Td	b.d.l.	b.d.l.	30.06	0.36	0.03	23.41	b.d.l.	0.01	2.66	9.02	b.d.l.	0.01	34.62	b.d.l.	100.19
D54	Zn-Td	b.d.l.	b.d.l.	24.86	b.d.l.	7.35	38.05	b.d.l.	b.d.l.	1.72	1.62	b.d.l.	0.15	26.89	b.d.l.	100.66
D50	Zn-Td	b.d.l.	0.04	25.67	b.d.l.	7.09	41.95	b.d.l.	b.d.l.	9.84	0.86	b.d.l.	0.07	13.78	b.d.l.	99.32
D52	Zn-Td	b.d.l.	b.d.l.	25.56	b.d.l.	7.88	41.34	b.d.l.	b.d.l.	10.91	0.48	b.d.l.	0.06	13.22	b.d.l.	99.45
d267	Zn-Td	b.d.l.	b.d.l.	25.65	b.d.l.	7.20	41.42	b.d.l.	b.d.l.	5.74	0.33	b.d.l.	0.04	21.13	b.d.l.	101.51
D51	Zn-Tn	b.d.l.	b.d.l.	26.09	b.d.l.	7.74	41.57	b.d.l.	b.d.l.	13.51	0.94	b.d.l.	0.04	9.46	b.d.l.	99.35
d251	Dg	b.d.l.	0.07	22.28	0.04	1.51	76.77	b.d.l.	0.01	b.d.l.	0.51	b.d.l.	0.13	b.d.l.	0.01	101.34
d252	Dg	0.02	b.d.l.	22.41	0.03	1.52	74.36	b.d.l.	b.d.l.	b.d.l.	0.58	b.d.l.	0.10	b.d.l.	0.04	99.05

(Continues)

TABLE 2 (Continued)

Number	Mineral	Se	Hg	S	Pb	Zn	Cu	Ni	Co	As	Fe	Au	Ag	Sb	Te	Total
d253	Anilite	0.03	b.d.l.	23.14	0.03	1.22	73.67	b.d.l.	b.d.l.	b.d.l.	2.68	b.d.l.	0.18	b.d.l.	0.04	101.00
D23	Alt	0.03	b.d.l.	b.d.l.	62.04	b.d.l.	0.01	b.d.l.	b.d.l.	b.d.l.	0.01	b.d.l.	0.00	b.d.l.	37.46	99.55
D26	Alt	b.d.l.	b.d.l.	b.d.l.	62.33	b.d.l.	b.d.l.	b.d.l.	b.d.l.	b.d.l.	0.01	b.d.l.	0.00	b.d.l.	37.21	99.57
D30	Alt	0.01	b.d.l.	b.d.l.	61.82	b.d.l.	b.d.l.	b.d.l.	b.d.l.	b.d.l.	b.d.l.	b.d.l.	0.00	b.d.l.	37.87	99.69
D35	Alt	b.d.l.	b.d.l.	b.d.l.	61.26	b.d.l.	b.d.l.	b.d.l.	b.d.l.	b.d.l.	0.02	b.d.l.	0.00	b.d.l.	38.27	99.55
D24	Ptz	0.02	0.31	0.01	b.d.l.	b.d.l.	b.d.l.	b.d.l.	b.d.l.	b.d.l.	b.d.l.	17.05	48.61	b.d.l.	34.24	100.40
D29	Ptz	b.d.l.	0.39	0.01	b.d.l.	b.d.l.	b.d.l.	b.d.l.	b.d.l.	b.d.l.	b.d.l.	16.99	47.34	b.d.l.	34.71	99.58
D31	Ptz	b.d.l.	0.34	0.01	b.d.l.	b.d.l.	0.01	b.d.l.	0.01	b.d.l.	b.d.l.	17.07	49.39	b.d.l.	33.98	100.93
D25	Cav	0.01	0.27	b.d.l.	b.d.l.	b.d.l.	0.14	b.d.l.	b.d.l.	b.d.l.	b.d.l.	29.37	8.53	b.d.l.	60.82	99.42
D27	Cav	0.03	0.43	b.d.l.	b.d.l.	b.d.l.	0.14	b.d.l.	b.d.l.	b.d.l.	b.d.l.	30.56	8.76	b.d.l.	59.85	100.07
D28	Cav	0.02	0.41	0.01	b.d.l.	b.d.l.	0.13	b.d.l.	b.d.l.	b.d.l.	b.d.l.	30.03	8.66	b.d.l.	60.90	100.46
D32	Cav	0.01	0.42	b.d.l.	b.d.l.	b.d.l.	0.08	b.d.l.	0.01	b.d.l.	b.d.l.	30.10	8.71	b.d.l.	59.43	99.05
D33	Cav	0.05	0.41	0.01	b.d.l.	b.d.l.	0.14	b.d.l.	b.d.l.	b.d.l.	b.d.l.	29.02	8.70	b.d.l.	60.63	99.26
D34	Cav	b.d.l.	0.37	0.50	0.06	b.d.l.	0.09	0.01	0.01	b.d.l.	b.d.l.	28.53	8.34	b.d.l.	58.19	96.32
D42	Cav	0.02	0.35	0.26	b.d.l.	b.d.l.	0.12	b.d.l.	b.d.l.	b.d.l.	1.50	26.02	8.49	b.d.l.	55.90	92.89
18D6	Hes	0.24	b.d.l.	0.10	b.d.l.	b.d.l.	b.d.l.	b.d.l.	b.d.l.	b.d.l.	b.d.l.	b.d.l.	62.42	b.d.l.	37.09	100.11
18D6-1	Hes	0.27	b.d.l.	0.18	b.d.l.	b.d.l.	b.d.l.	b.d.l.	b.d.l.	b.d.l.	0.02	0.02	62.49	b.d.l.	36.67	99.95
18D7	Hes	b.d.l.	b.d.l.	0.13	b.d.l.	b.d.l.	b.d.l.	b.d.l.	b.d.l.	b.d.l.	0.01	0.05	62.16	b.d.l.	36.96	99.53
18D13	Hes	0.23	b.d.l.	0.12	0.17	b.d.l.	b.d.l.	b.d.l.	b.d.l.	b.d.l.	0.04	0.05	62.64	b.d.l.	37.68	101.45

Abbreviation: b.d.l., below detection limit.

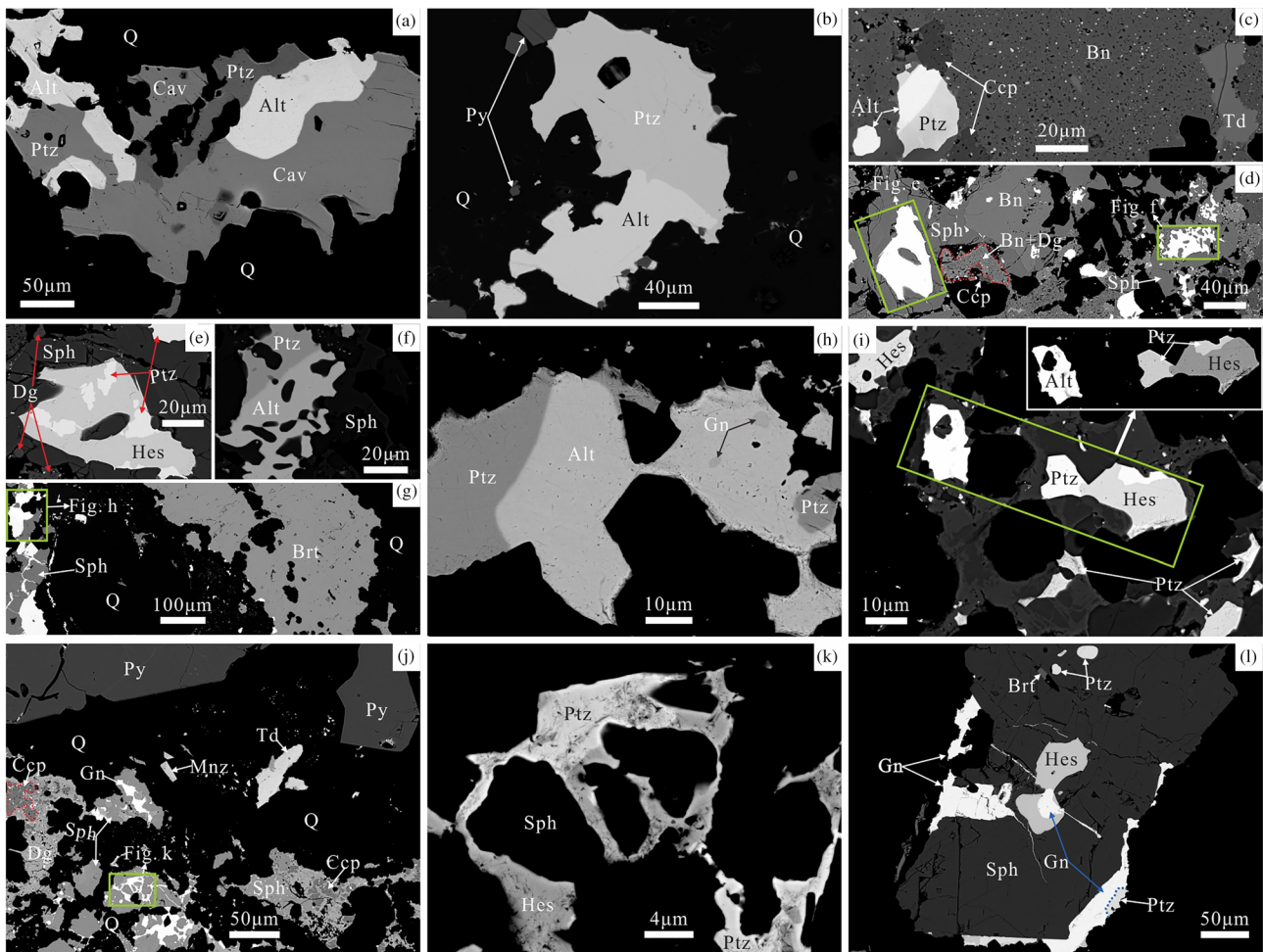


FIGURE 6 Backscattered electron images of tellurides in the quartz vein-type ores. (a) Intergrowths of petzite, calaverite and altaite in quartz. (b) Petzite coexisting with pyrite and altaite. (c–j) Intergrowths of petzite, calaverite, altaite and hessite, and occur as inclusions in bornite and sphalerite. (k) Petzite is replaced by hessite. (l) Intergrowths of hessite, petzite, galena and sphalerite, and sphalerite is filled by galena; Ptzt: petzite, Cav: calaverite, Alt: altaite, Q: quartz, Hes: hessite [Colour figure can be viewed at wileyonlinelibrary.com]

(Figure 5i); (e) bornite-galena-pyrite-chalcocopyrite-tetrahedrite (Figure 5k) etc.

4.3 | Native tellurium, gold and tellurides in quartz vein-type ores

The tellurides are mainly composed of Ag-, Au-Ag- and Pb-tellurides (Table 2, Figure 6). Previous studies also reported native tellurium, gold and calaverite (Chao et al., 2016; Wang et al., 2011). Intergrowths of gold, sylvanite, hessite, altaite and petzite are present in bornite, sphalerite, pyrite and quartz. Hessite usually occurs as tiny droplet inclusions in bornite and sphalerite (Figures 5 and 6). Observed intergrowth pairs include: 1) petzite-altaite-calaverite (Figure 6a); 2) petzite-pyrite-altaite (Figure 6b); 3) petzite-altaite-chalcocopyrite-bornite (Figure 6c); 4) petzite-hessite-sphalerite (Figure 6e); 5) petzite-altaite-galena (Figure 6h); 6) petzite-hessite (Figure 6k); 7) petzite-galena (Figure 6l) etc.

In fact, based on the EMPA result, the alleged ‘calaverite’ identified from microscopic observations is an Au-Ag telluride as shown in Figure 6, which approximates to sylvanite (AuAgTe_4) in chemical compositions. The general formula of ‘calaverite’ is $\text{Au}_{1.27}\text{Ag}_{0.69}\text{Te}_4$ and similar minerals have been reported from the Guilaizhuang gold deposit (Xu et al., 2014). Besides, compared with petzite (AuAg_3Te_2), the so-called ‘Ag-rich petzite’ in this paper, with the formula of $\text{Au}_{0.97}\text{Ag}_{5.01}\text{Te}_2$, contains relatively high contents of Ag (47.34–49.39 wt.%) as shown in Table 2, which may be produced by decomposition of petzite.

5 | DISCUSSION

5.1 | Constraints on the fugacity of $\text{S}_2(\text{g})$, $\text{Te}_2(\text{g})$ and $\text{O}_2(\text{g})$

Previous studies have shown that fugacity-fugacity diagrams are useful tools to investigate phase relations among intergrowth pairs and to

Luanling gold deposit. In the phase diagram of $\log fS_2(g)$ - $\log fTe_2(g)$ (Figure 7), chalcopyrite is only stable between the bornite + pyrrhotite-chalcopyrite and chalcopyrite-bornite + pyrite buffer and the $\log fS_2(g)$ varies from -15.7 to -6.5 , which can be used to limit the $\log fS_2(g)$. We cannot find any pyrrhotite in the Luanling gold deposit. Thus, the $\log fS_2(g)$ should be above the pyrrhotite-pyrite buffer and must be higher than -10.4 . Therefore, the $\log fS_2(g)$ is constrained from -10.4 to -6.5 (Figure 7).

5.1.2 | Fugacity of $Te_2(g)$

Tellurides are widely developed in the quartz vein-type ores, including calaverite, hessite, Au-Ag-telluride and altaite (Figure 6). Besides, native Te and Au have been reported by previous studies (Chao et al., 2016; Wang et al., 2011). Thus, the upper limit of $\log fTe_2(g)$ can be defined by Au-AuTe₂ equilibrium, at -7.9 (Afifi et al., 1988; Xu et al., 2014). The presence of hessite and the absence of argentite indicate that the $\log fTe_2(g)$ should be above the hessite-argentite buffer. According to the phases equilibrium of Po-Py, Ccp-Bn+Py and Ag₂Te-Ag₂Te, we constrain the lower limit of $\log fTe_2(g)$ to -13.68 . Therefore, the $\log fTe_2(g)$ can be constrained between -13.68 and -7.9 (Figure 7). In this fugacity range, tellurides minerals, except for calaverite that will be discussed later, can be closely associated with each other.

5.1.3 | Fugacity of $O_2(g)$

Most metal oxides are unstable with respect to tellurides and sulfides, consistent with the absence of oxides except for cassiterite, magnetite, or hematite from hypogene telluride ores. The above-mentioned three minerals can be used to construct the oxygen fugacity (Afifi et al., 1988a). Barite is widely developed in quartz vein-type ores and coexists with sulfides and tellurides in quartz vein-type ores, indicating that the $\log fO_2(g)$ should be above the barium sulfide-barite buffer and higher than -36.8 . Moreover, hematite is not present in the ores. According to the magnetite-hematite buffer, the upper limit of $\log fO_2(g)$ is estimated to be -31.1 . Therefore, the $\log fO_2(g)$ range can be defined as -36.8 to -31.1 (Figure 8), which locates between QFM-1.7 and QFM+4.0 (without constraints pressure) at $300^\circ C$.

5.2 | Deposition mechanism of gold

5.2.1 | Migration and precipitation mechanism of gold in altered rock-type ores

Available experimental studies and calculations have shown that gold can exist as Au¹⁺ and Au³⁺ in fluids. The former is the dominant oxidation state of Au in a majority of hydrothermal fluids, whereas the latter is stable only in oxidizing surface environments (Pokrovski, Tagirov, Schott, Bazarkina, et al., 2009; Pokrovski, Tagirov, Schott,

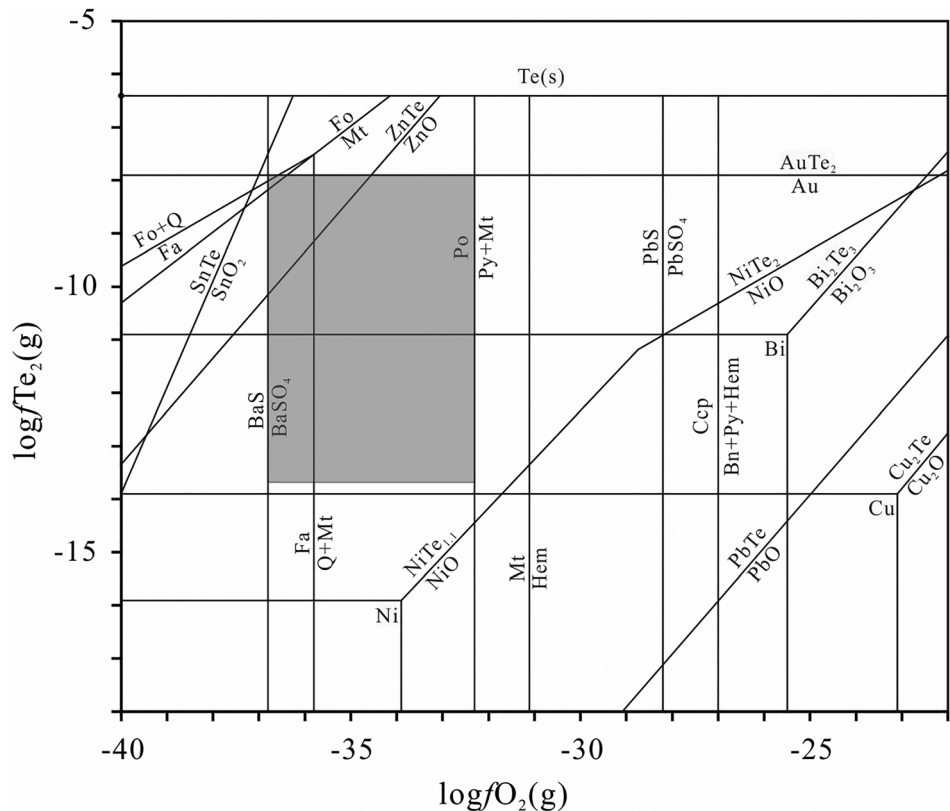
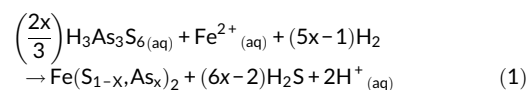


FIGURE 8 $\log fTe_2(g)$ - $\log fO_2(g)$ diagram showing the relative stability of some tellurides and their corresponding oxides as a function of their fugacities at $300^\circ C$

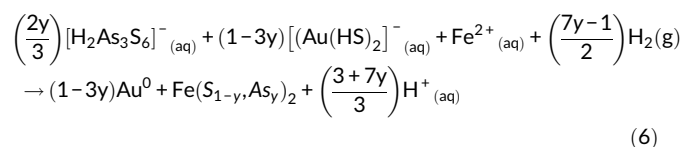
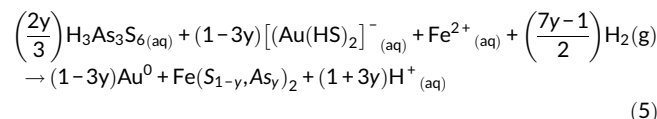
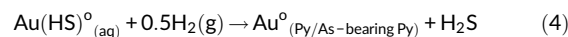
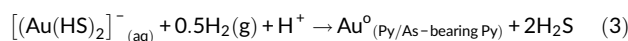
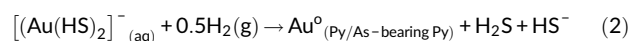
Hazemann, & Proux, 2009 and references therein). According to previous studies, gold is mainly transported in geological hydrothermal fluids as hydroxide, chloride and hydrogen sulfide complexes, including AuOH^0 , AuCl_2^- , AuHS^0 and $\text{Au}(\text{HS})_2^-$ (Seward, 1973, 1984; Stefánsson & Seward, 2004; Pokrovski et al., 2002, Pokrovski, Tagirov, Schott, Bazarkina, et al., 2009, Pokrovski, Tagirov, Schott, Hazemann, & Proux, 2009, 2014; Williams-Jones et al., 2009 and references therein). Under low to intermediate temperature, hydrogen sulfide complexes are dominant gold species in the majority of ore-forming fluids, with AuHS^0 predominating at acidic to intermediate pH solutions and $\text{Au}(\text{HS})_2^-$ at higher pH conditions in sulfide solutions (Pokrovski, Tagirov, Schott, Hazemann, & Proux, 2009; Seward, 1973; Stefánsson & Seward, 2004). However, at above 400°C, AuCl_2^- would be dominant in acidic sulfide solutions and $\text{Au}(\text{OH})^0$ predominates in neutral and alkaline sulfide solutions (Stefánsson & Seward, 2004; Williams-Jones et al., 2009). At low temperatures (<300°C), AuCl_2^- is the major carrier of gold in acidic chloride solutions, which hydrolyses to form $\text{Au}(\text{OH})^0$ and $\text{Au}(\text{OH})_2^-$ in neutral and alkaline chloride solutions (Stefánsson & Seward, 2003; Vlassopoulos & Wood, 1990 and references therein). Whereas at high (>400°C) temperatures, AuCl_2^- is the dominated carrier of gold in acidic chloride solutions, whereas $\text{Au}(\text{OH})^0$ and $\text{Au}(\text{OH})_2^-$ predominate in neutral and alkaline chloride solutions (Stefánsson & Seward, 2003, 2004; Williams-Jones et al., 2009 and references therein). Based on the mineralization assemblages in the Luanling gold deposit, the ore-forming fluid relevant to altered rock-type ores in this study should be a sulfide hydrothermal system and $\log f_{\text{S}_2}(\text{g})$ ranges from -10.4 to -6.5. Combining with estimated temperature (~300°C) and sulfur fugacity, we proposed that $\text{Au}(\text{HS})_2^-$ and AuHS^0 are the major speciations of gold-bearing complexes in the ore-forming fluid.

Sulfides, especially Au-bearing arsenian pyrite, are widely developed in the altered-type ores. In the $\log f_{\text{S}_2}(\text{g})$ - $\log f_{\text{Te}_2}(\text{g})$ phase diagram (Figure 7), the range of $\text{S}_2(\text{g})$ fugacity is relatively limited, which indicates that sulfides were precipitated rapidly from ore fluids under reducing conditions (Xu et al., 2014). Gold generally occurs as an invisible phase in pyrite and arsenian pyrite and probably exists as nano-particles in sulfides or ionic gold in their crystal lattice of the Luanling deposit, which is consistent with the occurrence of gold in the Carlin-type deposits (Deditius et al., 2014; Heitt et al., 2003; Large et al., 2009; Simon, Huang, et al., 1999, Simon, Kesler, & Chryssoulis, 1999 and reference therein). In addition, the iron of the Fe-bearing sulfides, in Carlin-type gold deposits, is considered to derive from the ferriferous carbonaceous surrounding rocks (Su et al., 2008 and reference therein). The Luanling gold deposit is hosted by the iron-rich trachyandesite-andesite of the Paleoproterozoic (1.80~1.75Ga) Xiong'er Group (Zhao et al., 2004). Previous studies have shown that arsenic generally substitutes sulfur in arsenian pyrite due to the similarity of their crystallochemical properties, especially in reducing environments (Deditius et al., 2014; Pokrovski et al., 2014 and reference therein). Therefore, the arsenian pyrite should be the result of interaction between Au-bearing complexes and the iron-rich wall rock and formed through the following reaction:

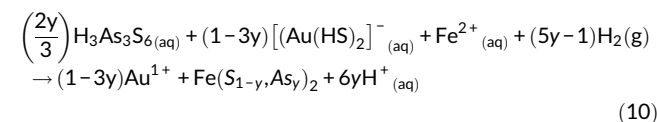
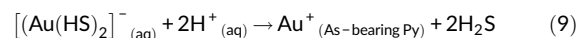
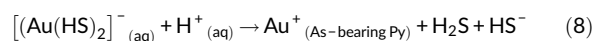
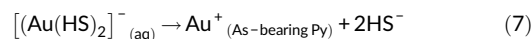


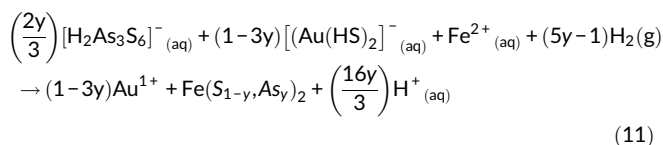
In addition, the formation of galena, sphalerite and chalcopyrite and tetrahedrite, which might postpone the pyrite precipitation (Xu et al., 2014). Furthermore, EMPA, laser ablation-inductively coupled plasma-mass spectrometry (LA-ICP-MS), X-ray absorption near-edge structure (XANES) and transmitted electron microscopy (TEM) measurements on oxidation status of gold in arsenian pyrite indicate that gold predominantly occurs as Au^+ , with little Au-bearing nanoparticles (our unpublished data). Thus, due to the changes of physicochemical conditions for ore-forming fluids, gold can be precipitated through the following chemical reactions in the gold-sulfides stage:

I Reactions for precipitation of free gold (Pokrovski et al., 2014; Simon, Huang, et al., 1999 and references therein)



II Reactions for precipitation of Au^+ in a vacancy position on an anion site in pyrite lattice (Pokrovski et al., 2014; Simon, Huang, et al., 1999 and references therein)

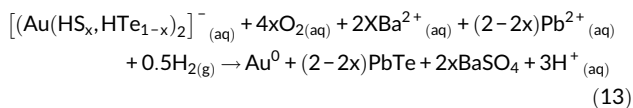
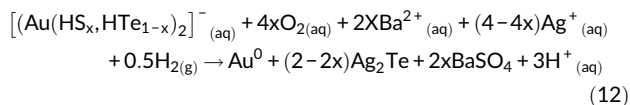




5.2.2 | Migration and precipitation mechanism of gold in quartz vein-type ores

Based on the detailed thermodynamic calculations, Zhang and Spay (1994) proposed that HTe^- , HTeO_3^- and Te_2^{2-} are the most important aqueous Te species in geological fluids. HTe^- occurs under reducing conditions (lower than the Ni-NiO buffer), whereas HTeO_3^- becomes a dominant speciation under oxidizing conditions (higher than the hematite-magnetite buffer), and Te_2^{2-} would be the major speciation between the Ni-NiO and hematite-magnetite buffers (Zhang & Spay, 1994 and references therein). Due to the precipitation of amounts of sulfides in the altered rock-type ores and input of the Te-rich hydrothermal fluid, the tellurium fugacity increased significantly with dramatic decreases of $\log f_{\text{S}_2(\text{g})}$ and pH in the remained hydrothermal fluids (Zhang & Spay, 1994; Xu et al., 2014). Besides, according to the estimated oxygen fugacity condition ($\log f_{\text{O}_2(\text{g})} = -36.8 \sim -31.1$, Figure 8) of this study, we propose that Te mainly exists as HTe^- with minor Te_2^{2-} and gold is mainly transported as $[\text{Au}(\text{HTe})_2]^-$, $[\text{HAu}(\text{HTe})_2]$ or $[\text{Au}(\text{HS}, \text{HTe})_2]^-$ in the hydrothermal fluid relevant to the quartz vein-type ores.

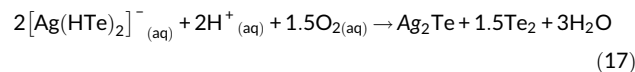
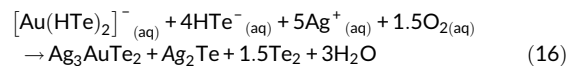
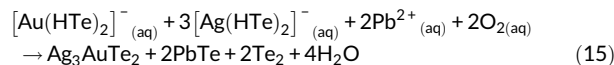
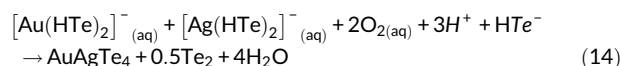
Combing the $\log f_{\text{Te}_2(\text{g})}$ - $\log f_{\text{O}_2(\text{g})}$ phase diagram (Figure 8) with the paragenetic associations (Figures 5 and 6), the oxygen fugacity is relatively high, and most sulfides and tellurides coexist with barite over a relatively large range of $\log f_{\text{O}_2}$ and $\log f_{\text{Te}_2}$ in the quartz vein-type ores. Under such oxidizing conditions, the partial sulfides are no longer stable and would be oxidized to SO_4^{2-} and Te would be released from the Au-Te or Au-S-Te complex and form tellurides, according to reactions as follows:



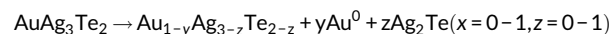
However, the sulfidation process in the altered-type ores and quartz vein-type ores would largely decrease the sulfur fugacity in ore-forming fluids. Therefore, the oxidization reaction shown above is limited for gold precipitation in the quartz vein-type ores (Liu et al., 2000; Xu et al., 2014).

Au-bearing telluride minerals occur in many gold deposits, implying that tellurides are important carriers of Au, Ag and PGE (Afifi et al., 1988a, 1988b; Ciobanu et al., 2006; Echmaeva & Osadchii, 2009; Xu et al., 2014 and references therein). In fact,

tellurides are the most important gold-bearing minerals in the quartz vein-type ores, including calaverite, petzite and hessite (Table 2). However, based on the EMPA results, the so-called 'calaverite' recognized from microscopic observations is indeed an Au-Ag tellurides and close to sylvanite (Figure 9), which is consistent with the phase relationships between tellurides and sulfides (Figure 7). Therefore, native gold cannot be associated with calaverite, because the Te fugacity is not enough to form calaverite (Xu et al., 2014). Besides, available experimental and calculations studies have shown that sylvanite (<354°C) and petzite (<304°C) are also stable at higher temperatures (Afifi et al., 1988a, 1988b; Cabri, 1965). Gold is likely complexed by Te in the form of $[\text{Au}(\text{HTe})_2]^-$ or $[\text{HAu}(\text{HTe})_2]$ as discussed above. Based on observations of the common intergrowths of petzite and/or hessite with sylvanite and or altaite in ores from the Luanling gold deposit, we proposed that most of the tellurides were contemporaneously precipitated from ore-forming fluids under relatively oxidized and acidic condition though the following reactions:



In addition, sylvanite and petzite would be unstable with decreasing temperature and decompose into hessite and calaverite at temperature below ~120°C (Afifi et al., 1988a; Cabri, 1965). In this study, gold precipitation is estimated at relative low temperature (~300°C). As petzite is closely associated with altaite, hessite and sylvanite (Figure 6), we propose that hessite, nature gold and Au-Ag tellurides with compositions on the tie lines among krennerite, sylvanite, petzite and hessite (Figure 9), are the products of the decomposition of sylvanite and petzite to a certain degree, with the following reactions (Xu et al., 2014):



The above decomposition process should be buffered by other stable tellurides such as PbTe, HgTe and NiTe₂. Similar phenomena have been reported by previous studies (Afifi et al., 1988a; Xu et al., 2014).

Furthermore, in Au-Ag-Te system, χ and γ phases are stable at high temperature and can decompose into the assemblages of hessite,

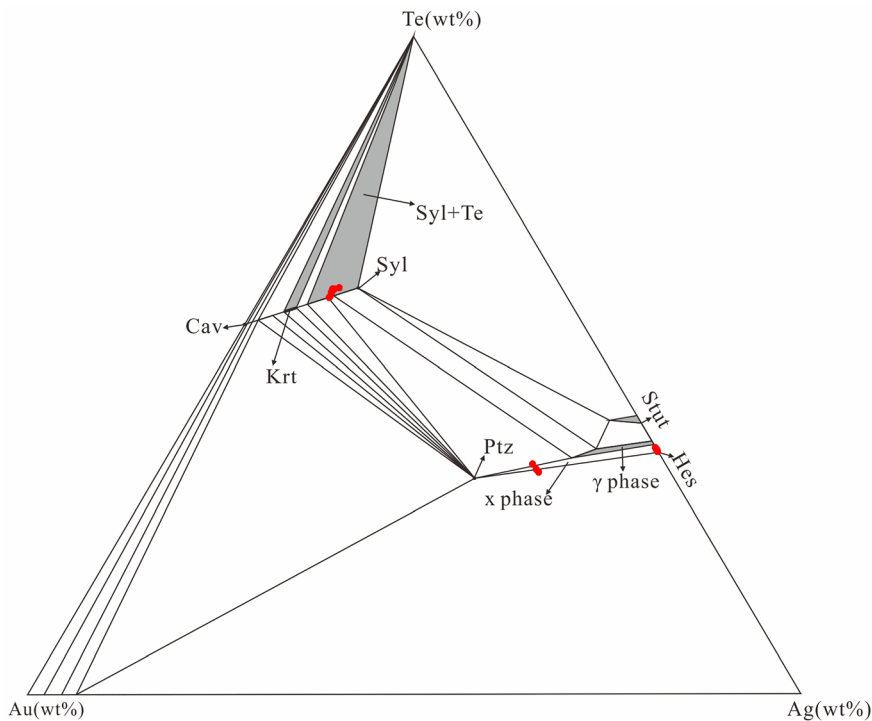


FIGURE 9 Ternary Au-Ag-Te showing the phase relationships among the Au-Ag tellurides at temperature between 120°C and 300°C diagram of system, modified from Zhang & Spry (1994); Krt = krennerite, Syl = sylvanite, Stut = stützite [Colour figure can be viewed at wileyonlinelibrary.com]

petzite, krennerite, stützite and sylvanite at temperature below ~50°C and ~120°C, respectively. (Afifi et al., 1988a; Cabri, 1965). Based on the plotted dots on the lines among krennerite, sylvanite, petzite and hessite in the Figure 9, we proposed that the solid solutions might form through the decomposition of χ and γ phases (Cabri, 1965; Xu et al., 2014 and references therein). However, we cannot provide the decomposition reactions of the two phases for limited thermodynamic parameters.

5.2.3 | Genetic relationships of the altered rock- and quartz vein-type ores

As discussed above, $\text{Au}(\text{HS})_2^-$ and AuHS^0 were the major speciations of gold-bearing complexes in ore-forming fluid relevant to the altered rock-type ores, whereas gold was mainly transported as $[\text{Au}(\text{HTe})_2]^-$, $[\text{HAu}(\text{HTe})_2]$ or $[\text{Au}(\text{HS}, \text{HTe})_2]^-$ in ore-forming fluid relevant to the quartz vein-type ores. During the upward migration of hydrothermal fluids, the $\log f\text{S}_2(\text{g})$ and pH would be significantly decreased in the remaining ore-forming fluids due to the precipitation of amounts of sulfides in the altered rock-type ores (Zhang & Spay, 1994; Xu et al., 2014). With the addition of some new Te-rich magmatic hydrothermal fluids, the Te fugacity would dramatically increase in the remaining ore-forming fluids, with precipitation of tellurides as a consequence (Chen et al., 1999). Moreover, the altered rock-type ores usually occur along both sides of, and sometimes as inclusions in the quartz vein-type ores (Figure 3b). These observations indicate that the quartz vein-type ores were slightly preceded by the altered rock-type ores. Besides, the Au-bearing arsenian pyrite in the altered rock-type ores has not experienced significant tectonic modification and is not filled

or enclosed by tellurides (Figure 5). These observations indicate that the ore-forming fluids relevant to the altered rock- and the quartz vein-type ores were from the same source and continuously evolved.

6 | CONCLUSIONS

In order to better understand the ore-forming process for altered rock- and quartz vein-type of ores in the Luanling gold deposit, we constructed fugacity-fugacity diagrams of phase equilibria among sulfides, tellurides and oxides via systematic thermodynamic calculations. Our study provides a simplified method to explain the ore-forming process for the diversity of gold mineralization.

The fugacity of $\text{S}_2(\text{g})$, $\text{O}_2(\text{g})$ and $\text{Te}_2(\text{g})$ played significant roles in the different types of gold mineralization in the Luanling gold deposit. The ore-forming fluid carried large amounts of S, As, Te and Au, and gold was mainly complexed by S and Te in terms of $[\text{Au}(\text{HS})_2]^-$, $[\text{Au}(\text{HTe})_2]^-$, and $[\text{Au}(\text{HS}, \text{HTe})_2]^-$. In the ore-forming fluid relevant to altered rock-type ores, $[\text{Au}(\text{HS})_2]^-$ is a dominant carrier of gold. Deposition of gold resulted from sulfidation of the nearby Fe-rich trachyandesite-andesite along the two sides of the main fault in the deposit and then formed the altered-type ores. During the sulfidation process, gold was liberated from the Au-S complexes during the reaction between sulfur in the hydrothermal fluids and iron in the trachyandesite-andesite. Gold occurs as ionic gold in the crystal lattice of pyrite and arsenian pyrite, and nano-particles of gold in the sulfides.

Due to the obvious decrease of sulfur fugacity for the sulfidation in the wall rock and addition of the Te-rich fluid, the Te fugacity would evidently increase and $[\text{Au}(\text{HTe})_2]^-$ and $[\text{Au}(\text{HS}, \text{HTe})_2]^-$ are the major carriers of gold in the ore-forming fluid relevant to quartz vein-

type ores. Under this condition, the relatively high oxygen fugacity can oxidize the partial residual sulfides into sulfate minerals such as barite. In addition, gold was primarily precipitated from the ore-forming fluids in the forms of main sylvanite, petzite, Au-Ag-tellurides, and minor native gold. According to phase relations among tellurides, sylvanite and petzite would decompose into native gold, hessite and more stable Au-Ag-tellurides with decreasing of temperatures. Based on comprehensive study, we proposed that the ore-forming fluids relevant to the altered rock- and the quartz vein-type ores were from the same source and continuously evolved.

ACKNOWLEDGEMENTS

We are grateful to Dr. Weiwei Chao to provide data of fluid inclusions in this study. Dr. Wengang Xu is thanked for his help during thermodynamic calculation analyses. Sincere thanks are extended to Dr. Xiaochun Li, Associate Professor Alexandra Yang Yang and Professor Wei Terry Chen for their constructive and valuable comments which greatly contributed to the improvement of the manuscript. This work is supported by the National Key Research and Development Program of China (Grant No. 2016YFC0600106) and the National Natural Science Foundation of China (Grant Nos. 41373046 & 41402047). This is contribution No.IS-2750 from GIGCAS.

CONFLICT OF INTEREST

The authors declare that there is no conflict of interest whatsoever with regard to the following manuscript submitted to Geological Journal for publication: 'Mineralization of the Luanling gold deposit in the southern margin of the North China Craton: Insights from mineralogy and mineral chemistry of sulfides, tellurides and oxides.'

ORCID

Lei Meng  <https://orcid.org/0000-0003-0782-3520>

Tai-Ping Zhao  <https://orcid.org/0000-0003-2392-898X>

REFERENCES

- Affifi, A. M., Kelly, W. C., & Essene, E. J. (1988a). Phase relations among tellurides, sulfides, and oxides; Pt. II. Applications to telluride-bearing ore deposits. *Economic Geology*, 83(2), 395–404. <https://doi.org/10.2113/gsecongeo.83.2.395>
- Affifi, A. M., Kelly, W. C., & Essene, E. J. (1988b). Phase relations among tellurides, sulfides, and oxides; I. Thermochemical data and calculated equilibria. *Economic Geology*, 83, 377–394. <https://doi.org/10.2113/gsecongeo.83.2.377>
- Archibald, S. M., Migdisov, A. A., & Williams-Jones, A. E. (2002). An experimental study of the stability of copper chloride complexes in water vapor at elevated temperatures and pressures. *Geochimica et Cosmochimica Acta*, 66, 1611–1619. [https://doi.org/10.1016/S0016-7037\(01\)00867-5](https://doi.org/10.1016/S0016-7037(01)00867-5)
- Bao, Z. W., Sun, W. D., Zartman, R. E., Yao, J. M., & Gao, X. Y. (2016). Recycling of subducted upper continental crust: constraints on the extensive molybdenum ore mineralization in the Qinling-Dabie orogen. *Ore Geology Reviews*, 81(2), 451–465.
- Barin, I. (1989). *Thermochemical Data of Pure Substances*. Pappelallee 3, D-69469 Weinheim, Federal Republic of Germany: WILEY-VCH Verlag GmbH. 1739 pp.
- Barton, J. P., & Skinner, B. (1979). Sulfide mineral stabilities. In H. L. Barnes (Ed.), *Geochemistry of Hydrothermal Ore Deposits* (pp. 278–403). John Wiley & Sons.
- Cabri, L. J. (1965). Phase relations in the Au-Ag-Te systems and their mineralogical significance. *Economic Geology*, 60, 1569–1606. <https://doi.org/10.2113/gsecongeo.60.8.1569>
- Chao, W. W., Ye, H. S., Tian, Y., Liu, Y. W., Lu, D. Y., Wang, P., ... Zhang, X. K. (2016). Re-Os isotopic dating of molybdenite from Luanling gold deposit in Xiong'er mountain ore concentration area of western Henan Province and its geological significance. *Mineral Deposits*, 35(1), 103–116. (in Chinese with English abstract)
- Chen, C. H., Cao, Z. M., Hou, X. P., Shuai, D. Q., & Luo, Y. N. (1999). The distributive law and main minerogenic conditions of gold-telluride deposits in the world. *Journal of Chengdu University of Technology*, 26, 241–248. (in Chinese with English abstract)
- Chen, Y. J., & Fu, S. G. (1992). *Gold mineralization in West Henna*. Beijing: Seismological Press. (in Chinese)
- Chen, Y. J., Pirajno, F., & Qi, J. P. (2008). The Shangong gold deposit, Eastern Qinling Orogen, China: Isotope geochemistry and implications for ore genesis. *Journal of Asian Earth Sciences*, 33, 252–266. <https://doi.org/10.1016/j.jseaes.2007.12.002>
- Chen, Y. J., Pirajno, F., Qi, J. P., Li, J., & Wang, H. H. (2006). Ore geology, Fluid Geochemistry and Genesis of the Shangong Gold Deposit, Eastern Qinling Orogen, China. *Resource Geology*, 56, 99–116. <https://doi.org/10.1111/j.1751-3928.2006.tb00272.x>
- Ciobanu, C. L., Cook, N. J., & Spry, P. G. (2006). Preface-special issue: telluride and selenide minerals in gold deposits-how and why? *Mineralogy and Petrology*, 87, 163–169. <https://doi.org/10.1007/s00710-006-0133-9>
- Craig, J. R., & Barton, P. B. (1973). Thermochemical approximations for sulfosalts. *Economic Geology*, 68, 493–506. <https://doi.org/10.2113/gsecongeo.68.4.493>
- Deditius, A. P., Reich, M., Kesler, S. E., Utsunomiya, S., Chryssoulis, S. L., Walshe, J., & Ewing, R. C. (2014). The coupled geochemistry of Au and As in pyrite from hydrothermal ore deposits. *Geochimica et Cosmochimica Acta*, 140, 644–670. <https://doi.org/10.1016/j.gca.2014.05.045>
- Deditius, A. P., Utsunomiya, S., Renock, D., Ewing, R. C., Ramana, C. V., Becker, U., & Kesler, S. E. (2008). A proposed new type of arsenian pyrite: Composition, nanostructure and geological significance. *Geochimica et Cosmochimica Acta*, 72, 2919–2933. <https://doi.org/10.1016/j.gca.2008.03.014>
- Echmaeva, E. A., & Osadchii, E. G. (2009). Determination of the thermodynamic properties of compounds in the Ag-Au-Se and Ag-Au-Te systems by the EMF method. *Geology of Ore Deposits*, 51, 247–258. <https://doi.org/10.1134/S1075701509030076>
- Gao, X. Y., & Zhao, T. P. (2017). Late Mesozoic magmatism and tectonic evolution in the southern margin of the North China Craton. *Science China Earth Sciences*, 60, 1959–1975. <https://doi.org/10.1007/s11430-016-9069-0>
- Gao, X. Y., Zhao, T. P., Yuan, Z. L., Zhou, Y. Y., & Gao, J. F. (2010). Geochemistry and petrogenesis of the Heyu batholith in the southern margin of the North China block. *Acta Petrologica Sinica*, 26, 3485–3506. (in Chinese with English abstract)
- Guo, B., Zhu, L. M., Li, B., Gong, H. J., & Wang, J. Q. (2009). Zircon U-Pb age and Hf isotope composition of the Huashan and Heyu granite plutons at the southern margin of North China Craton: implications for geodynamic setting. *Acta Petrologica Sinica*, 25, 265–281. (in Chinese with English abstract)
- Heitt, D. G., Dunbar, W. W., Thompson, T. B., & Jackson, R. G. (2003). Geology and geochemistry of the Deep Star gold deposit, Carlin trend, Nevada. *Economic Geology*, 98, 1107–1135. <https://doi.org/10.2113/gsecongeo.98.6.1107>
- Holland, H. D. (1959). Some application of thermochemical data to problems of ore deposits I. Stability relations among oxides, sulfides,

- sulfates and carbonates of ore and gangue minerals. *Economic Geology*, 60, 1101–1166.
- Holland, H. D. (1965). Some application of thermochemical data to problems of ore deposits II. Mineral assemblages and the composition of ore-forming fluids. *Economic Geology*, 60, 1101–1166. <https://doi.org/10.2113/gsecongeo.60.6.1101>
- Hu, S. X., Lin, Q. L., Chen, Z. M., & Li, S. M. (1988). *Geology and Metallogeny of the Collision Belt between the North and the South China Plates*. Nanjing, 558p: Nanjing University Press. (in Chinese)
- Landtwing, M. R., Pettke, T., Halter, W. E., Heinrich, C. A., Redmond, P. B., Einaudi, M. T., & Kunze, K. (2005). Copper deposition during quartz dissolution by cooling magmatic hydrothermal fluids: The Bingham porphyry. *Earth and Planetary Science Letters*, 235, 229–243. <https://doi.org/10.1016/j.epsl.2005.02.046>
- Large, R. R., Danyushevsky, L., Hollit, C., Maslennikov, V., Meffre, S., Gilbert, S., ... Foster, J. (2009). Gold and trace element zonation in pyrite using a laser imaging technique: Implications for the timing of gold in orogenic and Carlin-style sediment-hosted deposits. *Economic Geology*, 104, 635–668. <https://doi.org/10.2113/gsecongeo.104.5.635>
- Li, S. R., & Santosh, M. (2014). Metallogeny and craton destruction: Records from the North China Craton. *Ore Geology Reviews*, 56, 376–414. <https://doi.org/10.1016/j.oregeorev.2013.03.002>
- Li, S. R., & Santosh, M. (2017). Geodynamics of heterogeneous gold mineralization in the North China Craton and its relationship to lithospheric destruction. *Gondwana Research*, 50, 267–292. <https://doi.org/10.1016/j.gr.2017.05.007>
- Liu, J. J., Zheng, M. H., Liu, J. M., & Su, W. C. (2000). Geochemistry of the La'erma and Qiongmo Au-Se deposits in the western Qinling Mountains, China. *Ore Geology Reviews*, 17, 91–111. [https://doi.org/10.1016/S0169-1368\(00\)00008-1](https://doi.org/10.1016/S0169-1368(00)00008-1)
- Liu, Y., Li, S. R., Santosh, M., Xu, H., Li, C. P., & Liu, S. (2019). Ore-forming physicochemical conditions of Te-gold deposits: A case study from the Guilaizhuang deposit, eastern North China. *Geological Journal*, 54(4), 2400–2418. <https://doi.org/10.1002/gj.3303>
- Lu, X. X., Yu, X. D., Yu, Z. P., Wang, Y. T., Xue, L. W., Ye, A. W., ... Jin, J. P. (2004). Minerogenesis of gold and its coupling with tectonics in Xiaqingling-Xiongershan region. *Gold Geology*, 10(1), 1–5. (in Chinese with English abstract)
- Mallika, C., & Sreedharan, O. M. (1988). Standard molar Gibbs energy of formation of MoTe_2 from emf measurements. *Journal of Chemical Thermodynamics*, 20, 769–775. [https://doi.org/10.1016/0021-9614\(88\)90062-6](https://doi.org/10.1016/0021-9614(88)90062-6)
- Mao, J. W., Xie, G. Q., Pirajno, F., Ye, H. S., Wang, Y. B., Li, Y. F., ... Zhao, H. J. (2010). Late Jurassic-Early Cretaceous granitoid magmatism in Eastern Qinling, central-eastern China: SHRIMP zircon U-Pb ages and tectonic implications. *Australian Journal of Asian Earth Sciences*, 57(1), 51–78. <https://doi.org/10.1080/08120090903416203>
- Mills, K. C. (1974). Thermodynamic Data for Inorganic Sulfides. In *Selenides and Tellurides* (p. 845). London: Butterworths.
- Pokrovski, G. S., Akinfiev, N. N., Borisova, A. Y., Zotov, A. V., & Kouzmanov, K. (2014). Gold speciation and transport in geological fluids: insights from experiments and physical-chemical modelling. *Geological Society, London, Special Publications*, 402, 9–70. <https://doi.org/10.1144/SP402.4>
- Pokrovski, G. S., Kara, S., & Roux, J. (2002). Stability and solubility of arsenopyrite, FeAsS , in crustal fluids. *Geochimica et Cosmochimica Acta*, 66, 2361–2378. [https://doi.org/10.1016/S0016-7037\(02\)00836-0](https://doi.org/10.1016/S0016-7037(02)00836-0)
- Pokrovski, G. S., Tagirov, B. R., Schott, J., Bazarkina, E. F., Hazemann, J. L., & Proux, O. (2009). An in situ X-ray absorption spectroscopy study of gold-chloride complexing in hydrothermal fluids. *Chemical Geology*, 259, 17–29. <https://doi.org/10.1016/j.chemgeo.2008.09.007>
- Pokrovski, G. S., Tagirov, B. R., Schott, J., Hazemann, J. L., & Proux, O. (2009). A new view on gold speciation in sulfur-bearing hydrothermal fluids from in situ X-ray absorption spectroscopy and quantum-chemical modelling. *Geochimica et Cosmochimica Acta*, 73, 5406–5427. <https://doi.org/10.1016/j.gca.2009.06.007>
- Richards, J. P. (2011). Magmatic to hydrothermal metal fluxes in convergent and collided margins. *Ore Geology Reviews*, 40, 1–26. <https://doi.org/10.1016/j.oregeorev.2011.05.006>
- Robie, R. A., & Hemingway, B. S. (1995). Thermodynamic properties of minerals and related substances at 298.15 K and 1 bar (10^5 Pascals) pressure and at higher temperatures. *U.S. Geological Survey Bulletin*, 2131, 461–461.
- Robie, R. A., Seal, R. R., & Hemingway, B. S. (1994). Heat capacity and entropy of bornite (Cu_5FeS_4) between 6 and 760 K and the thermodynamic properties of phases in the system Cu-Fe-S. *Canadian Mineralogist*, 32, 945–956.
- Seal, R. R. II, Robie, R. A., Barton, P. B. Jr., & Hemingway, B. (1992). Superambient heat capacities of synthetic stibnite, berthierite, and chalcostibite: revised thermodynamic properties and implications for phase equilibria. *Economic Geology*, 87, 1911–1918. <https://doi.org/10.2113/gsecongeo.87.7.1911>
- Seward, T. M. (1973). Thio complexes of gold and the transport of gold in hydrothermal ore solutions. *Geochimica et Cosmochimica Acta*, 37, 379–399. [https://doi.org/10.1016/0016-7037\(73\)90207-X](https://doi.org/10.1016/0016-7037(73)90207-X)
- Seward, T. M. (1984). The transport and deposition of gold in hydrothermal systems. In R. P. Foster (Ed.), *Gold'82* (pp. 165–181). Rotterdam: A. A. Balkema.
- Simon, G., & Essene, E. J. (1996). Phase Relations among Selenides, Sulfides, Tellurides, and Oxides: I. Thermodynamic Properties and Calculated Equilibria. *Economic Geology*, 91, 1183–1208. <https://doi.org/10.2113/gsecongeo.91.7.1183>
- Simon, G., Huang, H., Penner-Hahn, J. E., Kesler, S. E., & Kao, L. S. (1999). Oxidation state of gold and arsenic in gold-bearing arsenian pyrite. *American Mineralogist*, 84, 1071–1079. <https://doi.org/10.2138/am-1999-7-809>
- Simon, G., Kesler, S. E., & Chryssoulis, S. (1999). Geochemistry and Textures of Gold-Bearing Arsenian Pyrite, Twin Creeks, Nevada: Implications for Deposition of Gold in Carlin-Type Deposit. *Economic Geology*, 94, 405–422. <https://doi.org/10.2113/gsecongeo.94.3.405>
- Simon, G., Kesler, S. E., & Essene, E. J. (1997). Phase Relations among Selenides, Sulfides, Tellurides, and Oxides II. Applications to Selenide-Bearing Ore Deposit. *Economic Geology*, 92, 468–484. <https://doi.org/10.2113/gsecongeo.92.4.468>
- Stefánsson, A., & Seward, T. M. (2003). The stability of chloridogold (I) complexes in aqueous solutions from 300 to 600 °C and 500 to 1800 bar. *Geochimica et Cosmochimica Acta*, 67, 4559–4576. [https://doi.org/10.1016/S0016-7037\(03\)00391-0](https://doi.org/10.1016/S0016-7037(03)00391-0)
- Stefánsson, A., & Seward, T. M. (2004). Gold(I) complexing in aqueous sulfide solutions to 500 °C at 500 bar. *Geochimica et Cosmochimica Acta*, 68, 4121–4143. <https://doi.org/10.1016/j.gca.2004.04.006>
- Su, W. C., Xia, B., Zhang, H. T., Zhang, X. C., & Hu, R. Z. (2008). Visible gold in arsenian pyrite at the Shuiyindong Carlin-type gold deposit, Guizhou, China: Implications for the environment and processes of ore formation. *Ore Geology Reviews*, 33, 667–679. <https://doi.org/10.1016/j.oregeorev.2007.10.002>
- Takács, Á., Molnár, F., Turi, J., Mogessie, A., & Menzies, J. C. (2017). Ore mineralogy and fluid inclusion constraints on the temporal and spatial evolution of a high-sulfidation epithermal Cu-Au-Ag deposit in the Recsk ore complex, Hungary. *Economic Geology*, 112, 1461–1481. <https://doi.org/10.5382/econgeo.2017.4517>
- Tang, K. F., Li, J. W., Selby, D., Zhou, M. F., Bi, S. J., & Deng, X. D. (2013). Geology, mineralization, and geochronology of the Qianhe gold deposit, Xiongershan area, southern North China Craton. *Mineralium Deposita*, 79, 729–747.
- Vlassopoulos, D., & Wood, S. A. (1990). Gold speciation in natural waters: I. Solubility and hydrolysis reactions of gold in aqueous solution.

- Geochimica et Cosmochimica Acta*, 54, 3–12. [https://doi.org/10.1016/0016-7037\(90\)90189-R](https://doi.org/10.1016/0016-7037(90)90189-R)
- Wang, J. X., Du, H. C., Liu, X. H., Zhang, Z. M., & Zhang, Y. W. (2011). The Ore Mineralogy Characteristics and Genetic Significance of Luanling Gold Deposit, Henan Province. *Gold Science and Technology*, 19(6), 12–17. (in Chinese with English abstract)
- Williams-Jones, A. E., Bowtell, R. J., & Migdisov, A. A. (2009). Gold in Solution. *Elements*, 5, 281–287. <https://doi.org/10.2113/gselements.5.5.281>
- Xiao, E., Hu, J., Zhang, Z. Z., Dai, B. Z., Wang, Y. F., & Li, H. Y. (2012). Petrogeochemistry, zircon U-Pb dating and Lu-Hf isotopic compositions of the Haoping and Jinshanmiao granites from the Huashan complex batholith in eastern Qinling Orogen. *Acta Petrological Sinica*, 28(12), 4031–4046. (in Chinese with English abstract)
- Xu, W. G., Fan, H. R., Hu, F. F., Santosh, M., Yang, K. F., Lan, T. G., & Wen, B. J. (2014). Gold mineralization in the Guilaizhuang deposit, southwestern Shandong Province, China: Insights from phase relations among sulfides, tellurides, selenides and oxides. *Ore Geology Reviews*, 56, 276–291. <https://doi.org/10.1016/j.oregeorev.2013.06.010>
- Xu, X. S., Griffin, W. L., Ma, X., O'Reilly, S. Y., He, Z. Y., & Zhang, C. L. (2009). The Taihua group on the southern margin of the North China craton: further insights from U-Pb ages and Hf isotope compositions of zircons. *Mineralogy and Petrology*, 97, 43–59. <https://doi.org/10.1007/s00710-009-0062-5>
- Xue, L. W., Yuan, Z. L., Zhang, Y. S., & Qiang, L. Z. (1995). The Sm-Nd isotope age of Taihua Group in Lushan area and their implications. *Geochemica*, 24, 92–97. (in Chinese with English abstract)
- Yang, C. X., & Santosh, M. (2020). Ancient deep roots for Mesozoic world-class gold deposit in the north China craton: An integrated genetic perspective. *Geoscience Frontiers*, 11(1), 203–214. <https://doi.org/10.1016/j.gsf.2019.03.002>
- Young, C. A., Dahlgren, E. J., & Robins, R. G. (2003). The solubility of copper sulfides under reducing conditions. *Hydrometallurgy*, 68, 23–31. [https://doi.org/10.1016/S0304-386X\(02\)00166-4](https://doi.org/10.1016/S0304-386X(02)00166-4)
- Zajacz, Z., Seo, J. H., Candela, P. A., Piccoli, P. M., & Tossell, J. A. (2011). The solubility of copper in high-temperature magmatic vapors: A quest for the significance of various chloride and sulfide complexes. *Geochimica et Cosmochimica Acta*, 75, 2811–2827. <https://doi.org/10.1016/j.gca.2011.02.029>
- Zhang, X. M., & Spay, P. G. (1994). Calculated Stability of Aqueous Te Species, Calaverite, and Hesseite at Elevated Temperatures.pdf. *Economic Geology*, 89, 1152–1166. <https://doi.org/10.2113/gsecongeo.89.5.1152>
- Zhao, T. P., Meng, L., Gao, X. Y., Jin, C., Wu, Q., & Bao, Z. W. (2018). Late Mesozoic felsic magmatism and Mo-Au-Pb-Zn mineralization in the southern margin of the North China Craton: A review. *Journal of Asian Earth Sciences*, 161, 103–121. <https://doi.org/10.1016/j.jseaes.2018.04.020>
- Zhao, T. P., Xu, Y. H., & Zhai, M. G. (2007). Petrogenesis and tectonic setting of the Paleoproterozoic Xiong'er Group in the southern part of the North China Craton: A review. *Geological Journal of China Universities*, 12, 191–206.
- Zhao, T. P., Zhai, M. G., Xia, B., Li, H. M., Zhang, Y. X., & Wan, Y. S. (2004). Study on the zircon SHRIMP ages of the Xiong'er Group volcanic rocks: constraint on the starting time of covering strata in the North China Craton. *Chinese Science Bulletin*, 49(22), 2342–2349. (in Chinese with English abstract)
- Zhou, H. Y., Sun, X. M., Fu, Y., Lin, H., & Jiang, L. Y. (2016). Mineralogy and mineral chemistry of Bi-minerals: Constraints on ore genesis of the Beiya giant porphyry-skarn gold deposit, southwestern China. *Ore Geology Reviews*, 79, 408–424. <https://doi.org/10.1016/j.oregeorev.2016.06.008>
- Zhou, H. Y., Sun, X. M., Wu, Z. W., Yang, T. J., Li, D. S., Ren, Y. Z., ... Yu, H. J. (2018). Mineralogy of Bi-sulfosalts and tellurides from the Yaoan gold deposit, southwest China: Metallogenic implications. *Ore Geology Reviews*, 98, 126–140. <https://doi.org/10.1016/j.oregeorev.2018.05.004>
- Zhu, R. X., Chen, L., Wu, F. Y., & Liu, J. L. (2011). Timing, scale and mechanism of the destruction of the North China Craton. *Science China Earth Sciences*, 41(5), 583–592. (in Chinese with English abstract)

SUPPORTING INFORMATION

Additional supporting information may be found online in the Supporting Information section at the end of this article.

How to cite this article: Meng L, Gao X-Y, Wu Q, Zhao T-P. Mineralization of the Luanling gold deposit in the southern margin of the North China Craton: Insights from mineralogy and mineral chemistry of sulfides, tellurides and oxides. *Geological Journal*. 2020;55:5831–5849. <https://doi.org/10.1002/gj.3660>